

A Framework for Uncertainty Propagation in 3D Shape Measurement using Laser Triangulation

Mahsa Mohammadikaji*, Stephan Bergmann*, Stephan Irgenfried*,
Jürgen Beyerer^{†*}, Carsten Dachsbacher* and Heinz Wörn*

*Karlsruhe Institute of Technology, Karlsruhe, Germany

[†]Fraunhofer Institute of Optronics, System Technologies and Image Exploitation IOSB, Karlsruhe, Germany

Email: {mahsa.mohammadikaji, stephan.bergmann, stephan.irgenfried, carsten.dachsbacher, woern}@kit.edu
juergen.beyerer@iosb.fraunhofer.de

Abstract—The analysis of measurement uncertainty is necessary in every measurement process. In this paper, we suggest an approach to categorize and model the dominant sources of uncertainty and study the probabilistic propagation of the uncertainties in a 3D inspection using laser line scanners. To each point of the measurement point cloud, we associate a covariance matrix describing the corresponding dispersion ellipsoid in the 3D space. The uncertainties can be analyzed for each desired laser and camera constellation and thus, the method can be applied in designing and optimizing laser scanner setups, reducing the effort of manually evaluating the setup in a trial and error approach. As a demonstration, the inspection of a cylinder head has been simulated using computer graphics and the estimated uncertainty metrics are visualized on the measured surface.

I. INTRODUCTION

Automatic product inspection is a growing requirement of today's manufacturing processes. An inspection is typically aimed at verifying a number of specifications to be within the allowed tolerances. Depending on the type of the product, surface properties and the allowed tolerances, different inspection methods can be applied. Common methods are typically optical or based on touch-trigger probes. Touch-trigger probes mounted on coordinate measuring machines (CMMs) provide high fidelity measurements with well-studied performance characteristics [1], but achieve much lower scan rates compared to optical sensors. On the other hand, optical methods are capable of fast contactless scanning of dense point clouds [2], but their performance can be affected by many environmental factors such as surface properties, illumination and sensor calibration quality, which play the role of uncertainty sources that propagate to the final measurement [3]. This resulting uncertainty directly limits the applicability of the inspection method, since one cannot inspect a surface when the tolerances are tighter than the measurement uncertainty.

To automate and improve the inspection process, sensor planning methods have been developed to optimize the scan view-points. The measurement uncertainty is an important factor to be optimized during the planning, alongside other goals such as complete target coverage. To this end, one needs a model describing how the uncertainty changes as the sensor view-point varies. Previous approaches typically rely on empirical models obtained by experimentally changing the sensor distance and orientation [4], [5]. These uncertainty

models are device dependent and only take a few parameters into account. Our focus is primarily to incorporate and model the most influencing sources of uncertainty to address the differences between devices, reduce the experimental work, and develop an analytic method for propagating the modeled uncertainties to the output measurement.

In this paper, we propose an uncertainty propagation framework for 3D shape measurement using laser line scanners, which are widely used optical inspection tools based on the principle of triangulation [6]. We categorize and model the effect of dominant sources of uncertainty on the measurement by suitable random variables, propose simple practical methods to assess their statistics in a real setup, and present a mathematical method to propagate the respective errors. The resulting calculated uncertainty is represented in terms of a 3×3 covariance matrix corresponding to a 3D ellipsoidal dispersion for each measured 3D point. This is particularly useful for designing and optimizing laser triangulation setups. In addition, the individual contribution of each source of uncertainty can be addressed, which provides us with an insight to recognize the dominating factors.

This paper is organized as follows: Upon reviewing the previous work in the next section, we give an overview of the model and methodology of the measurement using laser scanners in Section III. In sections IV, V and VI, we cover the statistical modeling and propagation of the dominant sources of uncertainty. Section VII presents the application of the method to a cylinder head inspection and demonstrates the results. Throughout the paper, bold lowercase letters denote vectors and uppercase letters correspond to matrices.

II. PREVIOUS WORK

In a number of previous works the uncertainty estimation is done in the calibration step by analyzing the uncertainty of reference point detection on the calibration object [3]. These uncertainties are then propagated to the 3D reconstruction or further, to the calculation of product properties such as width and flatness [7]. These methods are only based on the reference object and therefore do not account for the uncertainty induced by the surface properties of the inspected object.

Some authors have used experimental methods to model the systematic errors pertinent to the laser scanners in terms

of some geometrical setup parameters [2], [8]. In this paper, we intend to analyze the measurement uncertainties even when a systematic bias is not present or has been corrected.

Some works concern the uncertainty models for the purpose of sensor planning. Although the view-planning problem has a rich literature, the majority of works aim at optimizing the visibility constraints such as the optimum surface coverage with a minimal number of acquisitions. A few works use simple but different uncertainty models obtained experimentally, taking a few geometrical parameters into account [4], [5], [9]. Prieto et al. [5] suggest a model depending quadratically on the distance and exponentially on the orientation angles of the sensor. The model proposed by Scott [9] also grows quadratically with the distance but has an inverse cosine relation with the incident angle. The uncertainty model proposed by Mahmud et al. [4] depends only on the laser beam incidence angle. These models are empirically fitted by extensive experiments using a few pre-selected parameters. The considerable differences in the results also indicate that the models are device-dependent and therefore, the experiments should be repeated for every device.

One of our contributions to the previous works is to address the differences between devices, environments, and target surfaces by modeling the sensor and the dominant sources of uncertainty. The experimental work would then be reduced to only estimating the statistics of the random variables used in our uncertainty modeling, as we discuss in Section V. Analytically propagating the uncertainties leads to a mathematical function which can be used to evaluate the measurement uncertainty for different sensor configurations and can be applied to different sensor design and planning applications.

III. MEASUREMENT MODEL AND METHODOLOGY

Figure 1 illustrates the geometry of a laser scanner. The emitted laser plane creates an intersection curve on the object surface and a camera records images (similar to Fig. 2) as the object is moved along the x -axis. On the captured image, the peak intensities at the lateral center of the illuminated profile are extracted and processed to obtain a 3D point cloud of the object. In the rest of this section, we go through the mathematical derivation of the 3D point measurements.

We have modeled the camera with the well-known pin-hole camera model [10]. As shown in Eq. 1, this model defines the relation between the world coordinates of a measurement point (x_w, y_w, z_w) and the 2D coordinates (x_p, y_p) of its projection on the image plane.

$$\lambda \begin{bmatrix} x_p \\ y_p \\ 1 \end{bmatrix} = KP \begin{bmatrix} x_w \\ y_w \\ z_w \\ 1 \end{bmatrix} = \begin{bmatrix} f_x & s & c_x \\ 0 & f_y & c_y \\ 0 & 0 & 1 \end{bmatrix} [R \quad \mathbf{t}] \begin{bmatrix} x_w \\ y_w \\ z_w \\ 1 \end{bmatrix} \quad (1)$$

The projection matrix of a camera in this model is obtained by the multiplication of the matrix $K^{3 \times 3}$, containing the intrinsic calibration parameters (f_x, f_y, s, c_x, c_y) , and the matrix $P^{3 \times 4}$, built by the concatenation of a 3D rotation

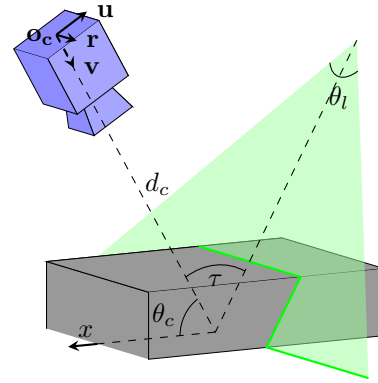


Fig. 1: Geometry of a laser scanner. \mathbf{o}_c is the origin of the camera coordinate frame spanned by the vectors \mathbf{u} , \mathbf{r} and \mathbf{v} . Angles τ and θ_l are referred to as triangulation and opening angle, respectively. d_c denotes the scan distance and θ_c is the angle between the camera axis and the horizon.

matrix R , and a translation vector \mathbf{t} . In this equation, R and \mathbf{t} determine the relative transformation of world to camera coordinate frame and λ is a scale factor. For simplicity, the skew parameter s is often considered to be zero.

The laser fan is typically produced by spreading the light of a laser beam through special lenses. This illuminated space can be modeled as part of a 3D plane in space using $\mathbf{x}^T \mathbf{n} = d$, where \mathbf{n} is the plane normal vector, \mathbf{x} is a world 3D point and d is a scalar.

The 3D coordinates of a 2D detected point on the image, fulfill both the laser plane equation as well as the camera projection model. Therefore, one can build a system of linear equations (Eq. 2) by adding the laser plane equation to the two independent linear equations obtained from Eq. 1 and recover the 3D coordinates (also known as triangulation [6]). Vectors \mathbf{r}^T , \mathbf{u}^T , and \mathbf{v}^T in Eq. 2 are the row vectors of the camera rotation matrix as depicted in Fig. 1, or equivalently $R^T = [\mathbf{r} \quad \mathbf{u} \quad \mathbf{v}]$, and t_i refers to an element of the translation vector $\mathbf{t} = [t_1 \quad t_2 \quad t_3]^T$.

$$\begin{bmatrix} \mathbf{r}^T - \mathbf{v}^T \frac{(x_p - c_x)}{f_x} \\ \mathbf{u}^T - \mathbf{v}^T \frac{(y_p - c_y)}{f_y} \\ \mathbf{n}^T \end{bmatrix} \begin{bmatrix} x_w \\ y_w \\ z_w \end{bmatrix} = \begin{bmatrix} \frac{(x_p - c_x)}{f_x} t_3 - t_1 \\ \frac{(y_p - c_y)}{f_y} t_3 - t_2 \\ d \end{bmatrix} \quad (2)$$

To keep the notation concise, the expression $A\mathbf{x} = \mathbf{b}$ is used to refer to Eq. 2. Thus, to obtain the 3D measurement point \mathbf{x} , one can build the matrix A and vector \mathbf{b} corresponding to the sensor geometry parameters and the 2D interest point (x_p, y_p) , and then compute

$$\mathbf{x} = A^{-1}\mathbf{b}. \quad (3)$$

IV. MEASUREMENT UNCERTAINTY

Due to the inevitable presence of uncertainties, every measurement is considered a random process. To make a metrological statement, one has to characterize the statistics of this randomness. According to the 'Guide to the Expression of Uncertainty in Measurement (GUM)' [11], methodologies for the uncertainty evaluation can be either based on the

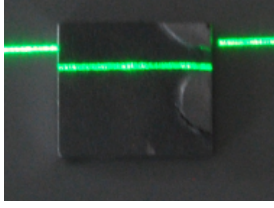


Fig. 2: Illuminating the target surface with a laser line

calculation of the statistics of repeated measurements (type A), or they are based on using the available information to propagate the uncertainties through the measurement (type B). Consequently, the method proposed in this paper is of type B.

The crucial requirement of the uncertainty propagation is the correct recognition and estimation of the uncertainty sources. However, since the sources can be numerous, it is tedious or even impossible to model every single factor. To simplify the modeling, we categorize the dominant sources of uncertainty into 3 main groups and model the induced perturbation of the measurement parameters caused by each group. Every source of uncertainty, regardless of its properties, can eventually influence the resulting measurement by perturbing some of the parameters in Eq. 2. With all the sources of uncertainty taken into account, the error-free form of Eq. 3 is replaced by the perturbed form

$$(\mathbf{x} + \delta\mathbf{x}) = (A + \delta A)^{-1}(\mathbf{b} + \delta\mathbf{b}). \quad (4)$$

Consequently, the first step is the modeling and estimation of input uncertainties δA and $\delta\mathbf{b}$, which we discuss in the next section. Later in Section VI, the derivation of the resulting measurement uncertainty $\delta\mathbf{x}$ will be studied.

V. UNCERTAINTY MODELING

In this section, we group the input parameters based on the part of the measurement they influence. The uncertainties induced on each group are statistically modeled by random variables. Further, we propose methods on how to estimate the statistics of the random variables in a real setup. This section is based on the assumption that the dominant uncertainty factors in a setup can be covered in the following categories and the effect of the other minor factors, such as temperature change, are negligible. Table I contains a summary of the uncertainty model parameters discussed in this section.

A. Laser Detection Uncertainty

First we consider the inaccuracies in the determination of the 2D coordinates of the detected laser line $\{x_p, y_p\}$ in the pixel domain. The typical approach is to localize the peak intensity in each column of the image using methods such as center of gravity or Gaussian approximation [12]. Many factors, such as the surface reflectance function and roughness (which leads to speckle noise), as well as the sensor noise, sampling, quantization effects, and the interpolation method can lead to uncertainties in the detection. The perturbed values are modeled by $\{x_p + e_{x_p}, y_p + e_{y_p}\}$, where e_{x_p} and e_{y_p} are assumed to be zero-mean Gaussian random variables.

A practical method to estimate the statistics (covariance matrix) of e_{x_p} and e_{y_p} is to illuminate a flat piece of the target surface by the laser to ensure that the laser forms a straight line (see Fig. 2). Then, an experimental image acquisition needs to be performed from a few different distances and viewing angles. Further, the peak intensity in each column will be interpolated. The uncertainties can be estimated based on the deviations of the detected peak location from the fitted line in each captured image. A conservative approach is to choose the maximum obtained deviation; however, one can build a more exact uncertainty model based on the sensor distance and orientation, which we leave as a future work.

B. Positioning Uncertainty

In cases where robots or other positioning devices are used to position the sensor, the uncertainty in the geometrical positioning must also be taken into account. The placement and angular uncertainties of positioning systems are usually reported by the manufacturer or they need to be estimated by experiment. In this section we study the incorporation of these uncertainties in positioning models to correctly analyze their effects. To the best of our knowledge, the work proposed by Scott [9] is the only work which has incorporated a pose uncertainty model in the planning; however, the propagation of the uncertainties to the output 3D measurement is not explicitly derived.

To allow a high degree of freedom in the view-planning, the laser and the camera are considered to be independently positioned and thus, they have their respective models.

1) *Camera*: As depicted in Fig. 3a, positioning uncertainties can lead to a transformation of the camera coordinate frame by a vector \mathbf{e}_o and some rotation matrix R_e . \mathbf{e}_o is modeled by three independent zero-mean Gaussians for each direction ($e_{o_x}, e_{o_y}, e_{o_z}$). The rotation matrix R_e has three degrees of freedom which must be parameterized according to the degrees of freedom of the positioning system. We have used the Euler angles to model the rotation with three independent random variables e_α, e_β and e_γ , which denote an uncertainty in pitch, roll and yaw angles, respectively. The noisy rotation angles are assumed to be zero-mean Gaussians, as well. Nevertheless, for each setup the parametrization

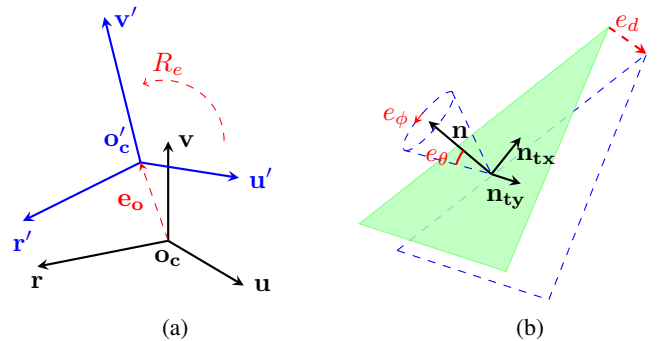


Fig. 3: Placement uncertainty models for camera coordinate frame (a) and laser plane (b).

TABLE I: Summary of uncertainty modeling for a laser line scanner

Group	Parameter	Error-Free Form	Perturbed Form	Random Variables
Laser detection uncertainty in pixel domain	horizontal	x_p	$x_p + e_{x_p}$	e_{x_p}
	vertical	y_p	$y_p + e_{y_p}$	e_{y_p}
Positioning uncertainty	camera rotation	R	$R_e R$	$e_\alpha, e_\beta, e_\gamma$
	camera position	\mathbf{t}	$R_e \mathbf{e}_o + \mathbf{t}$	$e_{o_x}, e_{o_y}, e_{o_z}$
	laser position	d	$d + e_d$	e_d
	laser normal	\mathbf{n}	see Sec. V-B2	e_θ, e_ϕ
Camera intrinsic uncertainty	focal length	f_x, f_y	$f_x + e_{f_x}, f_y + e_{f_y}$	e_{f_x}, e_{f_y}
	projection center	c_x, c_y	$c_x + e_{c_x}, c_y + e_{c_y}$	e_{c_x}, e_{c_y}

must be replaced by the suitable representation, that correctly describes the independent angles of the positioning system.

If the angular errors are small enough, one can make a linear approximation in the Euler rotation formula by approximating $\sin(a) \approx a$ and $\cos(a) \approx 1$ and ignoring the second and higher order multiplications of the angles. Holding this assumption, the approximated R_e can be represented by

$$R_e = \begin{bmatrix} 1 & e_\gamma & -e_\alpha \\ -e_\gamma & 1 & e_\beta \\ e_\alpha & -e_\beta & 1 \end{bmatrix}. \quad (5)$$

By applying the uncertainty model, the former error-free parameter set $\{R, \mathbf{t}\}$ in Eq. 2 will be replaced by the perturbed values $\{R_e R, R_e \mathbf{e}_o + \mathbf{t}\}$, according to the method of combining two rigid transformations [10].

2) *Laser*: As shown in Fig. 3b, the laser positioning uncertainties can either deviate the normal direction, or cause a movement of the plane. Although there are three degrees of freedom for the movement, only the component parallel to the normal vector is taken into account (e.i. e_d), since the other directions cause no changes in the geometrical equation of the plane. We also assume that the laser fan width is large enough compared to the object size, so as to cause negligible uncertainties by movement in other directions. Therefore, the parameter d in Eq. 2 will be perturbed by $d + e_d$, where e_d is modeled by a zero-mean Gaussian random variable.

Deviations of the normal direction are modeled by a cone parameterized by two independent random variables e_θ and e_ϕ . The variable e_θ is modeled by a zero-mean Gaussian whose standard deviation defines the cone half-angle. Given e_θ , the normal vector can equiprobably point to anywhere on the perimeter of the cone base. This is modeled by a uniform variable e_ϕ on the interval $[-\pi, \pi]$. Although e_ϕ has a high variance of $\frac{\pi^2}{3}$, as we later see in Section VI, it does not effect the measurement uncertainty. The deviations of the normal vector is therefore governed by e_θ .

Using this model, the perturbed normal vector will have the form $[\sin(e_\theta) \cos(e_\phi), \sin(e_\theta) \sin(e_\phi), \cos(e_\theta)]^T$. This vector is defined in the coordinate frame built by the vectors \mathbf{n}_{t_x} , \mathbf{n}_{t_y} , and \mathbf{n} . To obtain the perturbed normal in the reference frame, it needs to be multiplied by the rotation matrix $[\mathbf{n}_{t_x}, \mathbf{n}_{t_y}, \mathbf{n}]$.

The Gaussian random variables introduced in this section are assumed to be independent. They represent either an

angular or a positioning uncertainty. A practical way to estimate their standard deviations is to use the positioning and angular repeatability (equivalent of a type A uncertainty) of the manipulators used to position the laser and the camera.

C. Camera Intrinsic Calibration Uncertainty

The camera intrinsic parameters are extracted through calibration. Based on the accuracy of the calibration object and the suitability of the chosen model, calibration parameters can turn into an important source of uncertainty. We assume that the camera model contains no systematic error (or it has been compensated) and the variance and covariance of the uncertainty involved with the parameters are extracted during the calibration process using methods such as the one proposed by Leo and Paolillo [13]. In the pin-hole camera model used in this paper, the set $\{f_x, f_y, c_x, c_y\}$ contains the intrinsic values; however, the work can be extended to any suitable model, as long as the uncertainties of the parameters are extractable.

VI. UNCERTAINTY PROPAGATION FRAMEWORK

Based on the uncertainty modeling discussed in the previous section, the measurement parameters will be perturbed by a total number of 15 zero-mean random variables. These variables are described by their respective probability distributions if they are independent, or a group of variables are defined by a joint distribution if they are correlated. We also mentioned simple approaches on how to assign the statistics of the random variables in a real setup. The focus of this section is to propagate the input uncertainty distributions through the measurement and obtain the probability distribution of the resulting measurement ($\delta \mathbf{x}$ in Eq. 4).

This goal can be achieved in two ways. The first option is the Monte Carlo method which is based on repeated sampling of the input random variables to estimate the output probability density function. Although this method is useful for estimating complex output functions, the sampling space grows exponentially with the input dimension. Moreover, the process should be repeated in each constellation and for every measurement point, which is not feasible for the current application. Analytic methods, on the other hand, lead to mathematical expressions which can be evaluated efficiently for each desired constellation; however, they are often mathematically cumbersome. To overcome this difficulty, the model needs to be linearly approximated using Taylor series [14].

As seen in Eq. 3, the measurement point is obtained through the function $\mathbf{x} = A^{-1}\mathbf{b}$. To propagate the uncertainty using analytic methods, this function needs to be linearly approximated in terms of the uncertainty random variables. However, due to the presence of a matrix inversion, this leads to an improper function approximation. There exist upper and lower bounds for the error analysis in linear systems [15]; however, we are interested in obtaining the output probability distribution based on the input probabilities.

Haralick [14] proposes an interesting mathematical method of covariance propagation for parameter estimation in the cases where some desired parameter $\hat{\theta}$ is not obtained through an explicit function of the observations \mathbf{v} , but rather through an optimization of the form

$$\hat{\theta} = \underset{\theta}{\operatorname{argmin}} f(\mathbf{v}, \theta). \quad (6)$$

In this general form, f is a scalar function and \mathbf{v} denotes the noisy observation whose covariance matrix $\Sigma_{\mathbf{v}}$ is known. The goal is to obtain the covariance matrix of the resulting parameter $\Sigma_{\hat{\theta}}$. According to this method, by linearly approximating the gradient function $g(\mathbf{v}, \theta) = \frac{\partial f}{\partial \theta}$, the relation in Eq. 7 follows. This is based on the assumption that the second derivatives of f (partial derivatives of g) exist. For more details, the interested reader can refer to [14].

$$\Sigma_{\hat{\theta}} = \left(\frac{\partial g}{\partial \theta}\right)^{-1} \frac{\partial g^T}{\partial \mathbf{v}} \Sigma_{\mathbf{v}} \frac{\partial g}{\partial \mathbf{v}} \left(\left(\frac{\partial g}{\partial \theta}\right)^{-1}\right)^T \quad (7)$$

Once the measurement function is written in the form of Eq. 6, the modeled input covariance matrix can be translated to the measurement covariance matrix. Furthermore, the uncertainty propagation framework obtained in this way will be independent of the exact parametrization of the sources of uncertainty, but rather it can be applied to any suitable sensor model. To adapt the measurement function to that of [14], we rewrite Eq. 3 in the equivalent form of Eq. 8, which also avoids the matrix inversion term.

$$\hat{\mathbf{x}} = \underset{\mathbf{x}}{\operatorname{argmin}} (A\mathbf{x} - \mathbf{b})^T (A\mathbf{x} - \mathbf{b}) \quad (8)$$

In this context, $(A\mathbf{x} - \mathbf{b})^T (A\mathbf{x} - \mathbf{b})$ represents the scalar function f . The elements of A and \mathbf{b} contain the perturbed input parameters (i.e, the observations in Haralick's notation) whose uncertainties were modeled previously. $\hat{\mathbf{x}}$ is the resulting measurement point for which we seek the covariance matrix $\Sigma_{\hat{\mathbf{x}}}$. Consequently, by computing the second partial derivatives of the defined scalar function and building the input covariance matrix, the desired measurement covariance matrix results from Eq. 7.

As the partial derivative of our scalar function with respect to e_{ϕ} is zero, this uniform variable, as expected, does not effect the output uncertainties. Our input covariance matrix $\Sigma_{\mathbf{v}}$ is a 15×15 matrix, whose diagonal elements are the variances of the random variables and non-diagonal elements denote the covariances of each pair of them. We assume that all pairs of variables that are not in the same group (see

Section V) as well as the positioning variables defined in Section V-B are independent. The covariances within the other two groups (V-A and V-C) can be estimated during sample image acquisition and camera calibration, as discussed in the respective sections. This results in a 3×3 covariance matrix $\Sigma_{\hat{\mathbf{x}}}$ describing the dispersion of each 3D point.

VII. APPLICATION: INSPECTION OF A CYLINDER HEAD

The focus of this section is to provide a practical use case to demonstrate the applicability of the proposed framework. To this end, we consider the problem of scanning a cylinder head which moves on a conveyor belt. As seen in Fig. 4, the cylinder head CAD model is relatively complex. Therefore, planning methods can be particularly useful in generating optimized sensor view-points. Moreover, there are certain tolerances to be met during the inspection and it is of specific importance to guarantee and optimize the measurement uncertainty along other goals such as surface visibility.

Table II contains the assumed input standard deviations for the random variables, which are also considered to be uncorrelated. We have considered a value of 0.5mm as the standard deviation of $\{e_{o_x}, e_{o_y}, e_{o_z}, e_d\}$, which is a typical value for the position repeatability of industrial robots. For the rotational uncertainties $\{e_{\alpha}, e_{\beta}, e_{\gamma}, e_{\theta}\}$, a standard deviation of 0.01° is assumed. The laser detection uncertainty $\{e_{x_p}, e_{y_p}\}$ has been experimentally approximated to the value of 0.2px . Similarly, the calibration uncertainties $\{e_{f_x}, e_{f_y}, e_{c_x}, e_{c_y}\}$ are chosen based on the typical accuracy of intrinsic camera calibration. The assumed values have been used for demonstration purposes and must be set according to the sensor, setup, and the inspection object used.

A. Measurement Simulation & Demonstration of the Results

To apply the framework, we need the coordinates of the points measured in a desired constellation as the cylinder head is being moved. To this end, computer graphics methods have been applied to simulate the measurement. We have implemented a laser light source as a plugin to the Mitsuba renderer [16] which is further used to render images from the camera view. Fig. 5 displays a portion of a rendered image. Mitsuba

TABLE II: Assumed input standard deviations

Type of Uncertainty	Random Variables	σ
positioning	$e_{o_x}, e_{o_y}, e_{o_z}, e_d$	0.5 mm
rotation	$e_{\alpha}, e_{\beta}, e_{\gamma}, e_{\theta}$	0.01°
laser detection	e_{x_p}, e_{y_p}	0.2 px
calibration (focal length)	e_{f_x}, e_{f_y}	2 px
calibration (projection center)	e_{c_x}, e_{c_y}	0.5 px



Fig. 4: Cylinder head CAD model from two view-points

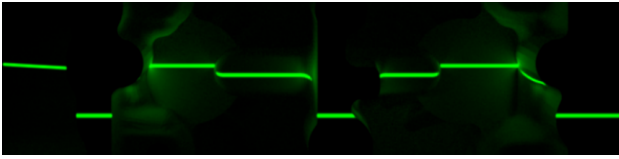


Fig. 5: Simulation of the cylinder head inspection

computes physically-based light transport and therefore it has been utilized to extract the ground-truth coordinates of the surface hit by the laser and captured by the camera. For each 2 millimeter movement of the cylinder head along the x -axis, an image has been rendered. The simulations have been performed at both sides of the cylinder head. In each image, the laser line is detected using the method of center of gravity [12] and the detected points are reconstructed using Eq. 2.

By applying the proposed framework, every measured point has been associated with a covariance matrix which can be used to evaluate the uncertainty along each desired direction. Fig. 6 displays the resulting uncertainties along the z -axis, so as to better illustrate the deviations from the nominal surface. This result has been calculated for the constellation in which $\theta_c = 90^\circ$, $\tau = 30^\circ$, $d_c = 200 \text{ mm}$ and $\theta_l = 90^\circ$, according to the setup geometry in Fig. 1.

By simulating the inspection in any desired setup constellation, the corresponding uncertainty metrics can be calculated. The optimum configuration can be achieved by integrating other quality metrics such as surface visibility and scan density, and efficiently searching the parameter space for positioning the laser and the camera. Moreover, this framework can be utilized in estimating the individual contribution of each source of uncertainty to the final measurement. To this end, one just needs to change the input covariance matrix by setting the variance and covariance of the non-intended variables to zero and evaluate the result. In the case of the assumed input uncertainties in Table II, more than 90% of the resulting uncertainty is induced by the positioning random variables e_{o_x} , e_{o_y} , e_{o_z} and e_{o_d} . This implies that the best practice to improve the setup in this case, is to improve the positioning system uncertainty, rather than investing time and money in better calibration methods or image processing algorithms.

VIII. CONCLUSION AND FUTURE WORK

In this paper, we studied a mathematical framework for statistical modeling and propagation of the uncertainties in a 3D inspection using laser scanners. By evaluating the efficiency of the measurement in each sensor configuration, the proposed approach can be applied to rapid prototyping of demanding laser triangulation setups, where the precision must meet certain tolerances. As the future work, we intend to use the proposed framework together with other optimization criteria such as visibility and scan resolution in a view-planning algorithm to optimize the cylinder head inspection.

ACKNOWLEDGMENT

The authors would like to kindly acknowledge the German Research Foundation (DFG) for financing this research.

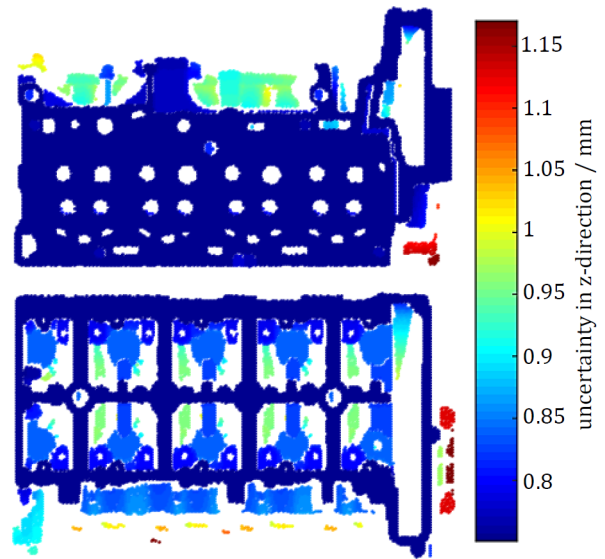


Fig. 6: Uncertainties (standard deviations) along the z -axis in the inspection of a cylinder head at both sides. The z -axis points out of the page.

REFERENCES

- [1] "Geometrical product specifications (GPS)–Acceptance and reverification tests for coordinate measuring machines (CMM)–Part 2: CMMs used for measuring linear dimensions," ISO 10360-2:2009, 2009.
- [2] H.-Y. Feng, Y. Liu, and F. Xi, "Analysis of digitizing errors of a laser scanning system," *Precision Engineering*, vol. 25, pp. 185–191, 2001.
- [3] A. Contri, P. Bourdet, and C. Lartigue, "Quality of 3d digitised points obtained with non-contact optical sensors," *CIRP Annals - Manufacturing Technology*, vol. 51, no. 1, pp. 443–446, 2002.
- [4] M. Mahmud, D. Joannic, M. Roy, A. Isheil, and J.-F. Fontaine, "3d part inspection path planning of a laser scanner with control on the uncertainty," *Computer-Aided Design*, vol. 43, no. 4, pp. 345–355, 2011.
- [5] F. Prieto, T. Redarce, P. Boulanger, and R. Lepage, "Cad-based range sensor placement for optimum 3d data acquisition," in *3-D Digital Imaging and Modeling, 1999. Proceedings. Second International Conference on*. IEEE, 1999, pp. 128–137.
- [6] J. Beyerer, F. P. León, and C. Frese, *Machine Vision: Automated Visual Inspection: Theory, Practice and Applications*. Springer, 2015.
- [7] J. Molleda, R. Usamentiaga, F. G. Bulnes, J. C. Granda, and L. Ema, "Uncertainty propagation analysis in 3-d shape measurement using laser range finding," *IEEE Transactions on Instrumentation and Measurement*, vol. 61, no. 5, pp. 1160–1172, 2012.
- [8] A. Isheil, J.-P. Gonnet, D. Joannic, and J.-F. Fontaine, "Systematic error correction of a 3d laser scanning measurement device," *Optics and Lasers in Engineering*, vol. 49, no. 1, pp. 16–24, 2011.
- [9] W. R. Scott, "Model-based view planning," *Machine Vision and Applications*, vol. 20, no. 1, pp. 47–69, 2009.
- [10] Y. Ma, S. Soatto, J. Kosecka, and S. S. Sastry, *An invitation to 3-d vision: from images to geometric models*. Springer Science & Business Media, 2012, vol. 26.
- [11] "Evaluation of Measurement data–Guide to the Expression of Uncertainty in Measurement," JCGM 100:2008, 2008.
- [12] R. B. Fisher and D. K. Naidu, "A comparison of algorithms for subpixel peak detection," in *Image Technology*, J. L. C. Sanz, Ed. Berlin, Heidelberg: Springer Berlin Heidelberg, 1996, pp. 385–404.
- [13] G. Di Leo and A. Paolillo, "Uncertainty evaluation of camera model parameters," in *2011 IEEE International Instrumentation and Measurement Technology Conference (I2MTC)*, pp. 1–6.
- [14] R. M. Haralick, "Propagating covariance in computer vision," in *Performance Characterization in Computer Vision*. Springer, 2000, pp. 95–114.
- [15] G. H. Golub and Van Loan, Charles F, *Matrix computations*, 3rd ed., ser. Johns Hopkins studies in the mathematical sciences. Baltimore and London: Johns Hopkins University Press, 1996.
- [16] J. Wenzel, "Mitsuba renderer," 2010, <http://www.mitsuba-renderer.org>.